Research Article | Vol. 28, No. 23 / 9 November 2020 / Optics Express 35321

Optics EXPRESS

Distributed-feedback blue laser diode utilizing a tunnel junction grown by plasma-assisted molecular beam epitaxy

G. Muziol,[1,*] M. Hajdel,[1] H. Turski,[1] K. Nomoto,[2] M. Siekacz,[1] K. Nowakowski-Szkudlarek,[1] M. Żak,[1] D. Jena,[2] H. G. Xing,[2] P. Perlin,[1,3] and C. Skierbiszewski[1]

[1]*Institute of High Pressure Physics Polish Academy of Sciences, Sokołowska 29/37, 01-142 Warsaw, Poland*
[2]*Cornell University, Ithaca, NY 14853, USA*
[3]*TopGaN Ltd, ul Sokołowska 29/37, 01-142 Warszawa, Poland*
[*]*gmuziol@unipress.waw.pl*

Abstract: In this paper, we demonstrate a novel approach utilizing tunnel junction (TJ) to realize GaN-based distributed feedback (DFB) laser diodes (LDs). Thanks to the use of the TJ the top metal contact is moved to the side of the ridge and the DFB grating is placed directly on top of the ridge. The high refractive index contrast between air and GaN, together with the high overlap of optical mode with the grating, provides a high coupling coefficient. The demonstrated DFB LD operates at λ=450.15 nm with a side mode suppression ratio higher than 35dB. The results are compared to a standard Fabry-Perot LD.

1. Introduction

Distributed feedback (DFB) laser diodes (LDs) are compact light emitters that offer high spectral purity, which makes them desirable for a wide range of applications such as telecommunication, sensing, metrology and atomic clocks [1,2]. DFB LDs are commercially available in the spectral range extending from red up to far infrared [2,3]. Surprisingly, in the violet, blue and green regimes the DFB LDs are not available, despite the commercial success of the III-nitride Fabry-Perot LDs [4,5].

The early attempts to manufacture violet DFB LDs were based on techniques well known from conventional III-V materials [6–8]. The gratings were buried inside the epitaxial structure and consisted of a material with a different refractive index. Such an approach allows for a high overlap between the optical mode and the grating. However, in case of III-N DFB LDs this approach provides limited coupling due to high lattice mismatch and low refractive index contrast between alloys. These reports showed low side mode suppression ratio (SMSR) below 20 dB [6–8]. The typical SMSR of conventional III-V DFB LDs is higher than 40 dB, which shows that the coupling strength to the grating in case of the early III-N devices is poor.

Recently, there has been much attention devoted to III-N DFB LDs with gratings fabricated after the epitaxial growth. Slight et al. fabricated deep patterns on the sides of the ridge, which allowed for a very high refractive index contrast between GaN and air [9]. The resulting SMSR in pulsed mode was 22 dB. Further development of this technique led to CW lasing and SMSR of 35 dB [10]. Kang et al. used laterally coupled SiN grating and achieved SMSR of 23 dB in pulsed mode [11,12]. Fabrication of grating by focused ion beam on fully processed commercially available green or cyan LD was proposed by Holguin-Lerma et al. [13,14]. The LDs showed SMSR of 37 dB. Zhang el al. presented a DFB LD with a patterned indium tin oxide cladding made on a semipolar crystal orientation [15]. The optical mode had a relatively high coupling with the grating, thanks to the transversal configuration. The resulting SMSR was 29 dB. As

#405994 https://doi.org/10.1364/OE.405994
Journal © 2020 Received 20 Aug 2020; revised 22 Oct 2020; accepted 26 Oct 2020; published 6 Nov 2020

Optics EXPRESS

can be seen, achieving a high SMSR in III-N DFB LDs, which is essential in many applications, remains a challenge.

In this paper we demonstrate a blue DFB LD with a very high coupling to the grating. The grating is placed on top of the epitaxial structure and is made by patterning of the ridge through its whole width, as shown in a concept art presented in Fig. 1. Such a design benefits from the high refractive index contrast between GaN and air and from the high overlap between optical mode and grating, due to the transversal coupling. The problem in such a design is the placement of the top metallization. The conductivity of the p-type layers in III-nitrides is the limiting factor. Due to high activation energy of the Mg dopant, the layers have to by highly doped, which decreases the mobility of carriers and results in resistivity of GaN:Mg on the order of 1 Ωcm [16,17]. Such a high resistivity excludes lateral conductivity in p-type layers. However, Malinverni et al. proposed to change the conductivity to n-type with the use of a tunnel junction (TJ), which enabled demonstration of a LD with metallization on the side and an air cladding [18]. The TJ is partially removed by means of dry etching. It is left only inside the ridge, which allows to form a current aperture. The n-type GaN:Si regrown on the structure supplies the current horizontally into the ridge and through the TJ. There is negligible tunneling outside of the ridge due to low Mg-doping in the layer below the TJ. Here we adopt this method in order to leave the ridge exposed to air, which allows us to exploit the high refractive index contrast between GaN and air and place the grating directly on top of the ridge.

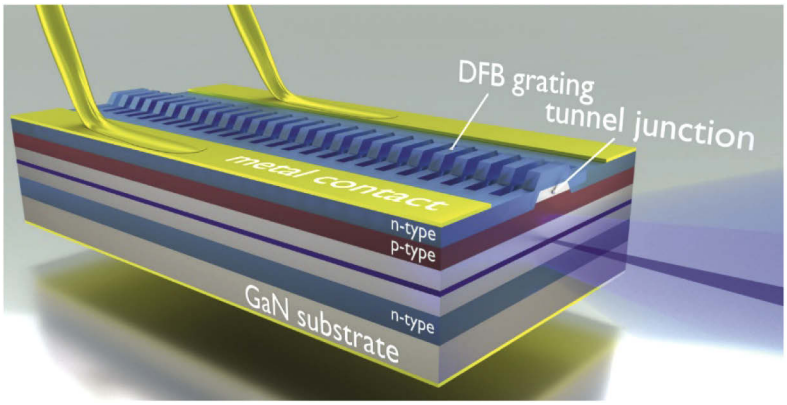

Fig. 1. Birds-eye view of the concept of a DFB LD with the metallization on the sides and the GaN/air grating on the top of the ridge.

The realization of such a design is enabled by use of a growth method, which allows to obtain highly conductive p-type without the hydrogen passivation issue. In metalorganic chemical vapor deposition (MOCVD), which is the commonly used technique to grow optoelectronic devices, the as-grown Mg-doped layers are passive and require post-growth annealing [16,19]. However, during the annealing process, the Mg-doped layers are required to be exposed to air to allow for hydrogen out-diffusion from the crystal [20,21]. Unfortunately, if the Mg-doped layers are buried below n-type layers, this process is blocked, due to low diffusivity of hydrogen in n-type material [22]. In the case of the demonstrated DFB LD structure the n-type material covers the sides and the top of the ridge and prevents hydrogen out-diffusion from the crystal. Therefore, the growth of the structure has been performed by plasma-assisted molecular beam epitaxy (PAMBE). With this technique the p-type conductivity in Mg-doped layers is active as-grown [23,24]. This is due to the hydrogen-free atmosphere during growth. Alternatively, ammonia MBE could be used, in which at the low growth temperatures, used in MBE, hydrogen does not incorporate into Mg-doped layers and p-type conductivity does not require activation [25,26].

Optics EXPRESS

2. Utilization of tunnel junction in the design of DFB LD

2.1. Structure detail

The growth was carried out by PAMBE in metal-rich conditions. Details of PAMBE growth can be found elsewhere [27]. High quality GaN crystals, obtained by the ammonothermal method were used [28]. The threading dislocation density of the substrate was in the order of 1×10^4 cm^{-2}. The schematics of the epitaxial structure of the DFB LD is presented in Fig. 2(a). It consists of a 700 nm $Al_{0.06}Ga_{0.94}N$:Si cladding, followed by a 100 nm GaN:Si. A high indium content $In_{0.08}Ga_{0.92}N$ waveguide is used to ensure high optical confinement [29] and prevent leakage of optical modes to GaN substrate [30]. Inside the waveguide there is a 25 nm wide $In_{0.17}Ga_{0.83}N$ QW, in which transitions between excited states ensure a high oscillator strength and optical gain [31]. The waveguide is followed by a 20 nm $Al_{0.15}Ga_{0.85}N$:Mg (Mg: 2×10^{19} cm^{-3}) electron blocking layer (EBL). The thickness of the GaN:Mg cladding between the EBL and TJ was chosen to be 70 nm, which is essential for this type of DFB LD The thickness of the GaN:Mg cladding is relatively thin compared to standard III-N LDs. It is chosen on purpose to allow for strong coupling of the optical mode with DFB grating on top of the ridge. In Section 2.2, the dependence of GaN:Mg thickness on coupling will be discussed. The TJ consisted of 60 nm $In_{0.02}Ga_{0.98}N$:Mg, 5 nm $In_{0.17}Ga_{0.83}N$:Mg, 5 nm $In_{0.17}Ga_{0.83}N$:Si and a 20 $In_{0.02}Ga_{0.98}N$:Si. The structure was capped with a 30 nm GaN:Si.

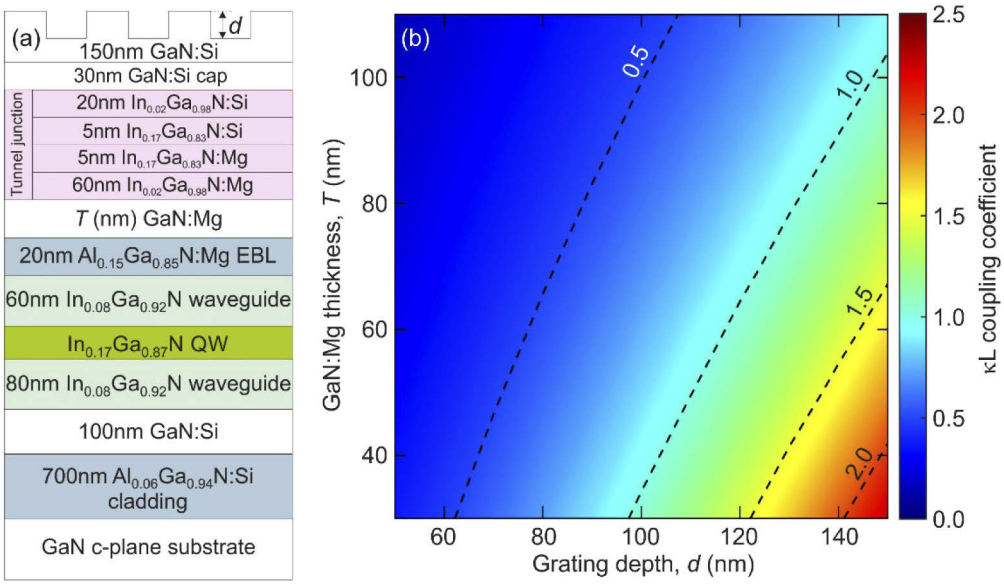

Fig. 2. (a) Schematics of the epitaxial structure. (b) Calculated dependence of κL on thickness of GaN:Mg layer and the grating depth.

Afterwards, a ridge was formed by reactive ion etching (RIE). The etching depth and ridge width were 130 nm and 2 µm, respectively. Importantly, the TJ was etched away everywhere except the ridge. This forms a current path, which ensures that the active region is pumped only below the ridge [18,32,33]. Next, a regrowth was performed. A 150 nm GaN:Si was grown on the whole surface. A 5th order DFB grating was made by electron beam lithography and RIE. The period of the grating was Λ=456 nm, the width of the top (unetched) and bottom (etched) parts were the same and equal to 228 nm. The etching depth was 100 nm, which is very shallow. After RIE, the sample was wet etched in TMAH at a temperature of 85°C for 15 minutes to smoothen the walls of the grating. The choice of the 5th order grating was motivated

Optics EXPRESS

by the interplay of the resonator length, coupling strength and the capability of realization of grating. A 5th order grating delivered reasonable κL (will be discussed in Section 2.2) and could be manufactured properly because of a relatively high period. Smaller grating is even more technologically challenging. Next, standard metal contacts to n-type GaN, consisting of 30 nm Ti, 60 nm Al, 40 nm Ni and 75 nm Au, were deposited on both sides of the device. The top metallization was not deposited on the ridge in order to leave it exposed to air. The resonator length was 700 μm and the facets were left uncoated.

2.2. Simulations of light coupling to DFB grating

To have an estimate of how the light traveling in the waveguide couples to the GaN/air grating on top of the ridge we have performed calculations in the following way. A two dimensional waveguide solver, CAMFR [34], was used to calculate the effective refractive index in two cases - etched and unetched parts of the grating. Next, the coupling coefficient has been calculated using the formula [35]:

$$\kappa L = 2m\frac{n_2 - n_1}{n_2 + n_1}$$

where κ is the coupling constant, L is the device length, m is the number of grating repetitions (a 5th order grating and a device length of 700 μm results in m=1535), n_1 and n_2 are the effective refractive indices of the etched and unetched parts of the grating, respectively.

The coupling coefficient in our design strongly depends on two parameters: (i) grating depth d, marked in Fig. 2(a) and (ii) distance between the waveguide and grating, the thickness T of the GaN:Mg was used to tune this parameter. The results of the calculations are presented in Fig. 2(b) as a two-dimensional map, which shows the influence of the two parameters. To achieve a strong coupling either the etching has to be deep or the thickness of GaN:Mg has to be low. We have decided to use the latter approach in the realization of the DFB LD because small etching depth of 100 nm ensures proper realization of the grating. The calculated κL and κ parameters for a 70 nm GaN:Mg, which was chosen for the experimental demonstration, were equal to 0.68 and 9.7 cm^{-1}, respectively. These values are slightly lower than those reported in Refs. [9,11]. However, the simplicity of fabrication of shallow grating ensures a good reproducibility over the whole resonator length and allows to obtain a high SMSR. It is important to stress that the placement of the grating on top of the ridge ensures a large coupling, even for such a small etching depth.

2.3. Electrical characterization of regrown GaN:Si

In order to keep the ridge exposed to air and supply current into the active region underneath, a GaN:Si layer is needed to be regrown after the ridge formation. This makes the GaN:Si not planar. During the standard operation of the LD with the metallization on the side of the ridge, the current needs to flow not only laterally, but also through the side walls of the ridge, if the mesa is deeper than the thickness of the regrown GaN:Si.

It is important, for the operation of a LD, that the current spreading throughout the length of the resonator is uniform. Therefore the GaN:Si regrown layer needs to be continuous on the walls of the ridge. Otherwise, inhomogeneities of electrical pumping of the active region might occur. Therefore, we will study here the electrical properties of the regrown material. To give an insight into the conductivity in the lateral part and through the walls of the ridge, three configurations will be compared, as shown in Fig. 3: (a) standard transmission line measurement (TLM), (b) resistivity between two metal pads on both sides of a shallow mesa and (c) deep mesa, in which the current needs to flow through GaN:Si grown on walls of the ridge. The etching depth of the ridge is 130 and 330 nm in case of the shallow and deep mesa, respectively. The thickness of the GaN:Si regrown layer is 150 nm. The measured resistivity is presented in Fig. 3(d). Remarkably, there is no significant difference in the resistivity between the fully planar GaN:Si and the sample with GaN:Si grown on walls of the ridge. The contact and GaN:Si resistivity were 5.6×10^{-5}

Optics EXPRESS

Ωcm^2 and 9.8×10^{-4} Ωcm, respectively. We have noticed a higher scatter of resistivities measured for the configurations with the ridge. This can be due to inhomogeneities of the GaN:Si grown on the edges and/or walls of the ridge. However, the fact that the resistivities in these two cases are comparable to the standard TLM suggests the part of the GaN:Si, grown on the walls, should be fairly continuous.

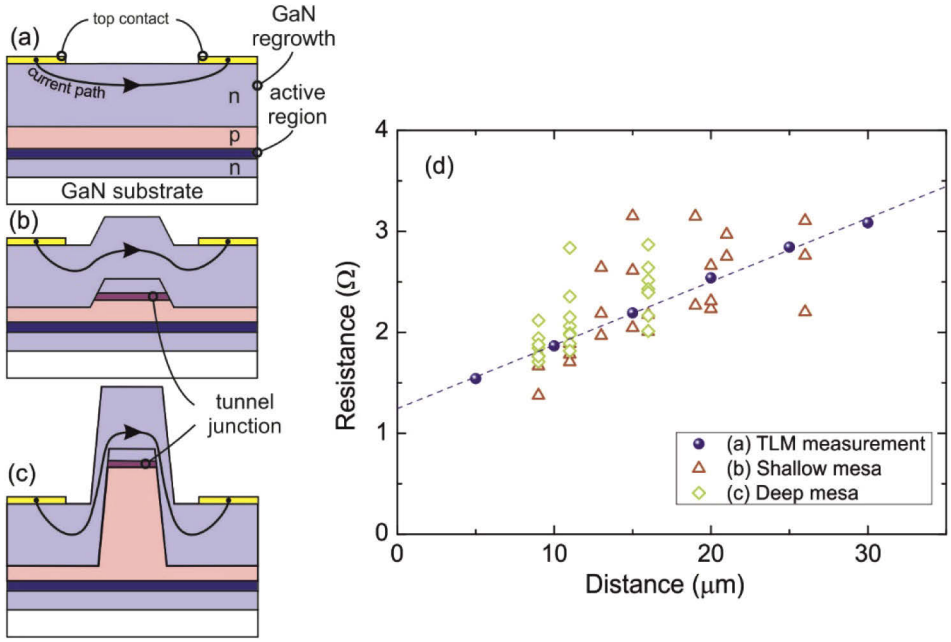

Fig. 3. Schematic design of the samples for electrical characterization of the regrown top GaN:Si layer: (a) standard TLM configuration, (b) shallow mesa and (c) deep mesa. (d) Dependence of resistance on distance between metal pads.

In the standard operating condition of the DFB LD, in which current is provided through the two metal pads, each 5 μm away from the ridge, and flow through the current aperture formed by the ridge, the resistance is estimated to be 0.5 Ω. Therefore, the voltage drop, due to moving the metallization away from the ridge, at an operating current of 150 mA, would be less than 0.1V. This is a small addition to the operating voltage, and can be accepted considering the benefits given by the exposed ridge.

3. Characterization of the DFB laser diode with tunnel junction

We have designed a DFB LD operating at λ=450 nm. Figure 4 presents scanning electron microscope picture of the processed device: (a) a view from the top of the ridge with grating and (b) a bird-eye view of the facet, ridge and metal pads on the sides of the ridge.

The DFB LDs were mounted in TO56 cans and operated in quasi-CW mode - the pulses were sufficiently long to keep the LD in an optically steady state. However, this resulted in a chirped spectrum due to heating. The pulse length was 1 ms and the duty cycle was up to 20%. Full CW operation was not achieved due to device overheating. The DFB LD is compared to a standard Fabry-Perot LD grown by PAMBE [36]. There are a few differences between the DFB LD and the Fabry-Perot LD. In the latter: (a) the thickness of GaN:Mg cladding is 500 nm (b) there is no TJ and (c) there is a standard Ni/Au metallization on top of the ridge. The LIV characteristics of a regular Fabry-Perot LD and DFB LD are presented in Figs. 5(a) and 5(b), respectively. The threshold current densities of the standard LD and DFB LD are 3.3 and 7.0 kA/cm^2, respectively.

Optics EXPRESS

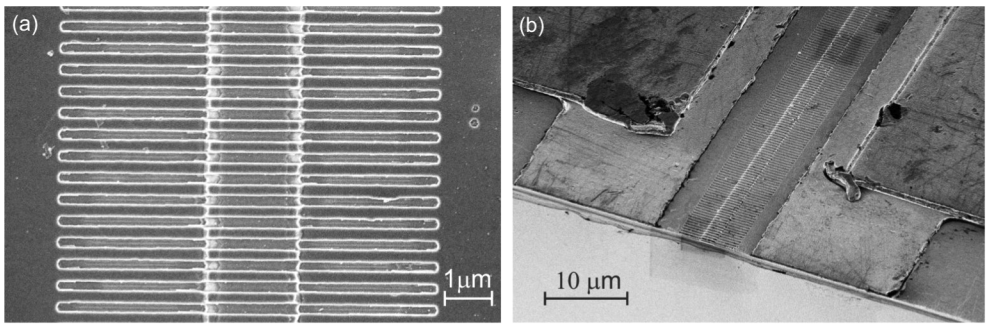

Fig. 4. Scanning electron microscope images of the fabricated DFB LD: (a) top view of the grating on the ridge and (b) the birds-eye view of the LD facet, ridge with grating and metallization on the sides.

This is a more than two-fold increase and it shows how much room for improvement is for the DFB LDs. Additionally, the slope efficiency decreased from 0.5 to 0.17 W/A. Both changes in threshold current density and slope efficiency point to an increase in the internal losses of the DFB LD. It is possible that the grating is not homogenous throughout the whole length of the ridge – this would lead to an increase in the internal losses.

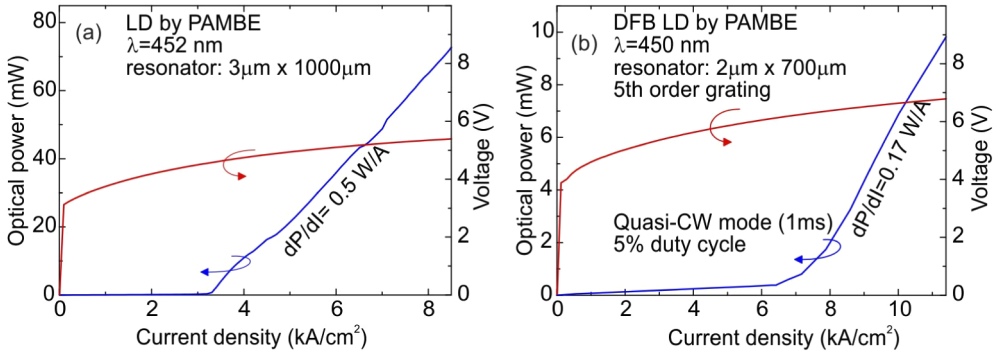

Fig. 5. Light-Current-Voltage characteristics of the: (a) standard Fabry-Perot LD operated in CW mode, (b) DFB LD operated in a quasi-CW mode.

The voltage at threshold of the DFB LD was 6.2 V, whereas in the case of the Fabry-Perot LD, at the same current density, the voltage was 5.2 V. This additional 1V is mainly due to the use of a TJ [37]. Recently, we have shown that the voltage drop on the TJ can be significantly reduced by engineering of the doping profile and piezoelectric polarization [38]. We expect that use of an optimized TJ, together with decrease of the threshold current density, will result in CW operation in the future.

The optical spectra below threshold of the Fabry-Perot LD and DFB LD are presented in Figs. 6(a) and 6(b), respectively. In case of the Fabry-Perot LD, clear longitudinal modes supported by the resonator can be observed. The spacing between the modes is 32 pm. The FWHM of each mode is ~10pm. In contrast, in the spectrum of the DFB LD there is one highly pronounced peak with a FWHM of 25 pm. The Fabry-Perot modes are also visible, however these are severely dampened compared to the single mode supported by the grating. The spacing between the Fabry-Perot modes is 45 pm. It is larger than in the Fabry-Perot LD case because of the shorter resonator length of the DFB LD (700 μm and 1000 μm for the DFB LD and Fabry-Perot LD, respectively).

Optics EXPRESS

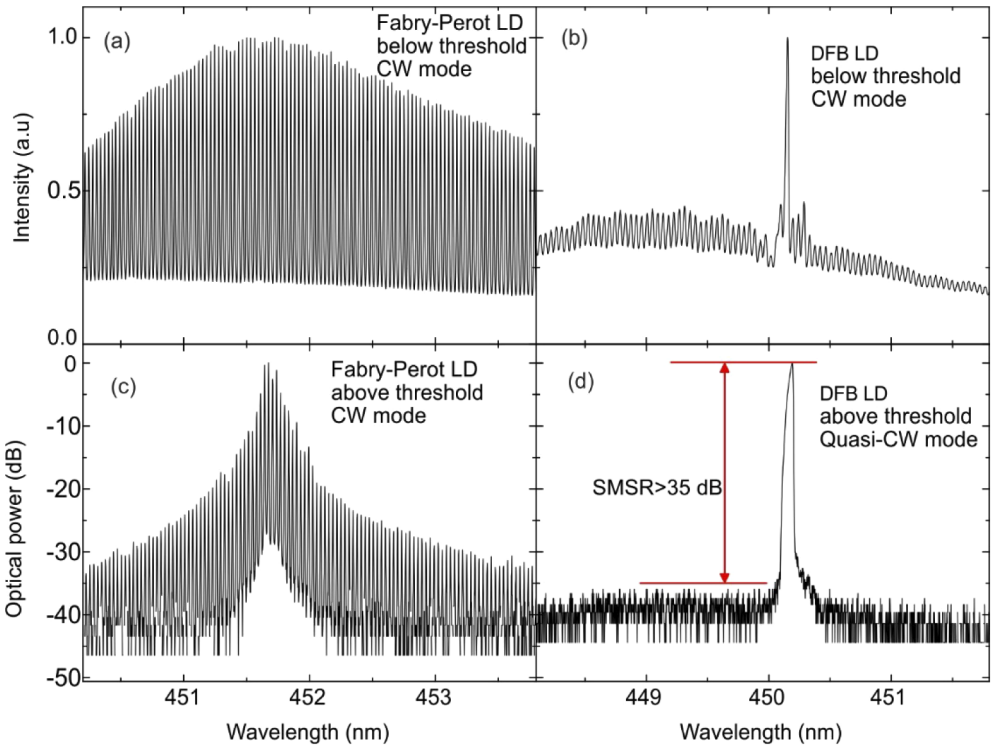

Fig. 6. Optical spectra of: (a) Fabry-Perot LD below threshold, (b) DFB LD below threshold, (c) Fabry-Perot LD above threshold and (d) DFB LD above threshold. Please note the logarithmic scale in (c) and (d). The broadening of the lasing mode in DFB LD is caused by the quasi-CW operation in which the spectrum is chirped due to heating.

The optical spectra above lasing threshold of the Fabry-Perot LD and DFB LD are presented in Figs. 6(c) and 6(d), respectively. In case of the Fabry-Perot LD clear longitudinal modes can be distinguished with a spacing of 32 pm. The FWHM of each mode is close to the limit of the spectrometer accuracy and is equal to 4 pm. In contrast, the DFB LD has only one peak with FWHM of 36 pm. The peak is asymmetrically broadened due to pulsed operation. During the pulse, the DFB LD heats up and its emission wavelength red-shifts. The spectrum is collected throughout the whole pulse width, therefore the resulting spectrum is chirped. It is expected that after the CW operation is obtained the peak will be symmetrical and narrower. Nevertheless, the achieved SMSR was above 35 dB, which is exceptionally high for a device operated in pulsed mode. This result is an order of magnitude better than other reported III-nitride DFB LDs operated in pulsed mode. Moreover, the achieved SMSR is comparable to values reported for CW operated devices. Such a high SMSR is a consequence of the high overlap of the optical mode with the grating placed on top of the ridge. We expect that after optimization, which will enable CW operation, the SMSR will improve greatly.

We will shortly discuss approaches to optimize the design of the DFB LD. Firstly, the possibility of generation of optical losses in the TJ has to be investigated. If the TJ is causing unwanted optical losses the composition of the InGaN QW inside the TJ can be decreased. This could strongly limit the band to band absorption. Secondly, the doping of the p-type layers can be optimized. Mg-doped layers are known to cause the major part of the optical losses in III-N LDs. The DFB LD design strongly differs from the conventional III-N LDs and requires a separate optimization process. Thirdly, the coupling of the optical mode with the grating can be increased.

Optics EXPRESS

This can be achieved by introduction of λ/4 shift [35], decrease of the grating order, increase of the duty cycle or increase of the resonator length. Additionally, any improvement in the grating quality and its uniformity is essential.

4. Conclusions

We have demonstrated a novel concept of a III-nitride distributed feedback laser diode with a high coupling of the optical mode to the grating. The grating was created by etching of GaN on top of the ridge. The high refractive index contrast between GaN and air, together with close vicinity of the grating and waveguide, resulted in high coupling. In order to form the grating on top of the ridge the metallization had to be moved to the side of the mesa. This was achieved by switching the conductivity to n-type with a tunnel junction. The devices were operated in quasi-CW and a high side mode suppression ratio of 35 dB was achieved. This result shows great promise in the realization of single mode III-N DFB LDs.

Funding

National Science Foundation (ECCS-1542081, MRI DMR-1631282, MRSEC DMR-1719875, RAISE TAQs 1839196); Narodowe Centrum Nauki (2019/35/D/ST3/03008, 2019/35/N/ST7/02968); Narodowe Centrum Badań i Rozwoju (LIDER/29/0185/L-7/15/NCBR/2016, LIDER/35/0127/L9/17/NCBR/2018); Fundacja na rzecz Nauki Polskiej (TEAMTECH POIR.04.04.00-00-210C/16-00).

Disclosures

The authors declare no conflicts of interest.

References

1. H. Kogelnik and C. V. Shank, "Coupled-Wave Theory of Distributed Feedback Lasers," J. Appl. Phys. **43**(5), 2327–2335 (1972).
2. D. R. Scifres, R. D. Burnham, and W. Streifer, "Distributed-feedback single heterojunction GaAs diode laser," Appl. Phys. Lett. **25**(4), 203–206 (1974).
3. L. Mahler, R. Köhler, A. Tredicucci, F. Beltram, H. E. Beere, E. H. Linfield, D. A. Ritchie, and A. G. Davies, "Single-mode operation of terahertz quantum cascade lasers with distributed feedback resonators," Appl. Phys. Lett. **84**(26), 5446–5448 (2004).
4. S. Nakamura, M. Senoh, S.-i. Nagahama, N. Iwasa, T. Yamada, T. Matsushita, H. Kiyoku, and Y. Sugimoto, "InGaN-Based Multi-Quantum-Well-Structure Laser Diodes," Jpn. J. Appl. Phys. **35**(Part 2, No. 1B), L74–L76 (1996).
5. S. Uchida, M. Takeya, S. Ikeda, T. Mizuno, T. Fujimoto, O. Matsumoto, G. Shu, T. Tojyo, and M. Ikeda, "Recent progress in high-power blue-violet lasers," IEEE J. Sel. Top. Quantum Electron. **9**(5), 1252–1259 (2003).
6. D. Hofstetter, R. L. Thornton, L. T. Romano, D. P. Bour, M. Kneissl, and R. M. Donaldson, "Room-temperature pulsed operation of an electrically injected InGaN/GaN multi-quantum well distributed feedback laser," Appl. Phys. Lett. **73**(15), 2158–2160 (1998).
7. A. C. Abare, M. Hansen, J. S. Speck, S. P. DenBaars, and L. A. Coldren, "Electrically pumped distributed feedback nitride lasers employing embedded dielectric gratings," Electron. Lett. **35**(18), 1559–1560 (1999).
8. S. Masui, K. Tsukayama, T. Yanamoto, T. Kozaki, S.-i. Nagahama, and T. Mukai, "CW Operation of the First-Order AlInGaN 405 nm Distributed Feedback Laser Diodes," Jpn. J. Appl. Phys. **45**(No. 46), L1223–L1225 (2006).
9. T. J. Slight, O. Odedina, W. Meredith, K. E. Docherty, and A. E. Kelly, "InGaN/GaN Distributed Feedback Laser Diodes With Deeply Etched Sidewall Gratings," IEEE Photonics Technol. Lett. **28**(24), 2886–2888 (2016).
10. T. J. Slight, S. Stanczyk, S. Watson, A. Yadav, S. Grzanka, E. Rafailov, P. Perlin, S. P. Najda, M. Leszczyński, S. Gwyn, and A. E. Kelly, "Continuous-wave operation of (Al,In)GaN distributed-feedback laser diodes with high-order notched gratings," Appl. Phys. Express **11**(11), 112701 (2018).
11. J. H. Kang, M. Martens, H. Wenzel, V. Hoffmann, W. John, S. Einfeldt, T. Wernicke, and M. Kneissl, "Optically Pumped DFB Lasers Based on GaN Using 10th-Order Laterally Coupled Surface Gratings," IEEE Photonics Technol. Lett. **29**(1), 138–141 (2017).
12. J. H. Kang, H. Wenzel, V. Hoffmann, E. Freier, L. Sulmoni, R. S. Unger, S. Einfeldt, T. Wernicke, and M. Kneissl, "DFB Laser Diodes Based on GaN Using 10th Order Laterally Coupled Surface Gratings," IEEE Photonics Technol. Lett. **30**(3), 231–234 (2018).

Optics EXPRESS

13. J. A. Holguin-Lerma, M. Kong, O. Alkhazragi, X. Sun, T. Khee Ng, and B. S. Ooi, "480-nm distributed-feedback InGaN laser diode for 10.5-Gbit/s visible-light communication," Opt. Lett. **45**(3), 742–745 (2020).
14. J. A. Holguín-Lerma, T. K. Ng, and B. S. Ooi, "Narrow-line InGaN/GaN green laser diode with high-order distributed-feedback surface grating," Appl. Phys. Express **12**(4), 042007 (2019).
15. H. Zhang, D. A. Cohen, P. Chan, M. S. Wong, S. Mehari, D. L. Becerra, S. Nakamura, and S. P. DenBaars, "Continuous-wave operation of a semipolar InGaN distributed-feedback blue laser diode with a first-order indium tin oxide surface grating," Opt. Lett. **44**(12), 3106–3109 (2019).
16. S. Nakamura, T. Mukai, M. Senoh, and N. Iwasa, "Thermal Annealing Effects on P-Type Mg-Doped GaN Films," Jpn. J. Appl. Phys. **31**(Part 2, No. 2B), L139–L142 (1992).
17. U. Kaufmann, P. Schlotter, H. Obloh, K. Köhler, and M. Maier, "Hole conductivity and compensation in epitaxial GaN:Mg layers," Phys. Rev. B **62**(16), 10867–10872 (2000).
18. M. Malinverni, C. Tardy, M. Rossetti, A. Castiglia, M. Duelk, C. Vélez, D. Martin, and N. Grandjean, "InGaN laser diode with metal-free laser ridge using n+-GaN contact layers," Appl. Phys. Express **9**(6), 061004 (2016).
19. H. Amano, M. Kito, K. Hiramatsu, and I. Akasaki, "P-Type Conduction in Mg-Doped GaN Treated with Low-Energy Electron Beam Irradiation (LEEBI)," Jpn. J. Appl. Phys. **28**(Part 2, No. 12), L2112–L2114 (1989).
20. Y. Kuwano, M. Funato, T. Morita, K. Yamashita, K. Yagi, M. Iwaya, T. Takeuchi, S. Kamiyama, and I. Akasaki, "Lateral Hydrogen Diffusion at p-GaN Layers in Nitride-Based Light Emitting Diodes with Tunnel Junctions," Jpn. J. Appl. Phys. **52**(8S), 08JK12 (2013).
21. W. Li, K. Nomoto, K. Lee, S. M. Islam, Z. Hu, M. Zhu, X. Gao, J. Xie, M. Pilla, D. Jena, and H. G. Xing, "Activation of buried p-GaN in MOCVD-regrown vertical structures," Appl. Phys. Lett. **113**(6), 062105 (2018).
22. R. Czernecki, E. Grzanka, R. Jakiela, S. Grzanka, C. Skierbiszewski, H. Turski, P. Perlin, T. Suski, K. Donimirski, and M. Leszczynski, "Hydrogen diffusion in GaN:Mg and GaN:Si," J. Alloys Compd. **747**, 354–358 (2018).
23. I. P. Smorchkova, E. Haus, B. Heying, P. Kozodoy, P. Fini, J. P. Ibbetson, S. Keller, S. P. DenBaars, J. S. Speck, and U. K. Mishra, "Mg doping of GaN layers grown by plasma-assisted molecular-beam epitaxy," Appl. Phys. Lett. **76**(6), 718–720 (2000).
24. A. Feduniewicz, C. Skierbiszewski, M. Siekacz, Z. R. Wasilewski, I. Sproule, S. Grzanka, R. Jakieła, J. Borysiuk, G. Kamler, E. Litwin-Staszewska, R. Czernecki, M. Boćkowski, and S. Porowski, "Control of Mg doping of GaN in RF-plasma molecular beam epitaxy," J. Cryst. Growth **278**(1-4), 443–448 (2005).
25. M. Malinverni, J.-M. Lamy, D. Martin, E. Feltin, J. Dorsaz, A. Castiglia, M. Rossetti, M. Duelk, C. Vélez, and N. Grandjean, "Low temperature p-type doping of (Al)GaN layers using ammonia molecular beam epitaxy for InGaN laser diodes," Appl. Phys. Lett. **105**(24), 241103 (2014).
26. A. Dussaigne, B. Damilano, J. Brault, J. Massies, E. Feltin, and N. Grandjean, "High doping level in Mg-doped GaN layers grown at low temperature," J. Appl. Phys. **103**(1), 013110 (2008).
27. C. Skierbiszewski, H. Turski, G. Muziol, M. Siekacz, M. Sawicka, G. Cywiński, Z. R. Wasilewski, and S. Porowski, "Nitride-based laser diodes grown by plasma-assisted molecular beam epitaxy," J. Phys. D: Appl. Phys. **47**(7), 073001 (2014).
28. R. Dwiliński, R. Doradziński, J. Garczyński, L. P. Sierzputowski, A. Puchalski, Y. Kanbara, K. Yagi, H. Minakuchi, and H. Hayashi, "Bulk ammonothermal GaN," J. Cryst. Growth **311**(10), 3015–3018 (2009).
29. G. Muziol, H. Turski, M. Siekacz, P. Wolny, S. Grzanka, E. Grzanka, P. Perlin, and C. Skierbiszewski, "Enhancement of optical confinement factor by InGaN waveguide in blue laser diodes grown by plasma-assisted molecular beam epitaxy," Appl. Phys. Express **8**(3), 032103 (2015).
30. G. Muziol, H. Turski, M. Siekacz, S. Grzanka, P. Perlin, and C. Skierbiszewski, "Elimination of leakage of optical modes to GaN substrate in nitride laser diodes using a thick InGaN waveguide," Appl. Phys. Express **9**(9), 092103 (2016).
31. G. Muziol, H. Turski, M. Siekacz, K. Szkudlarek, L. Janicki, M. Baranowski, S. Zolud, R. Kudrawiec, T. Suski, and C. Skierbiszewski, "Beyond Quantum Efficiency Limitations Originating from the Piezoelectric Polarization in Light-Emitting Devices," ACS Photonics **6**(8), 1963–1971 (2019).
32. M. Malinverni, D. Martin, and N. Grandjean, "InGaN based micro light emitting diodes featuring a buried GaN tunnel junction," Appl. Phys. Lett. **107**(5), 051107 (2015).
33. K. Gibasiewicz, A. Bojarska-Cieślińska, G. Muzioł, C. Skierbiszewski, S. Grzanka, A. Kafar, P. Perlin, S. Najda, and T. Suski, "InGaN blue light emitting micro-diodes with current path defined by tunnel junction," Opt. Lett. **45**(15), 4332–4335 (2020).
34. "CAMFR (CAvity Modelling FRamework)", retrieved 06 August 2020, 2020, http://camfr.sourceforge.net.
35. L. A. Coldren, S. W. Corzine, and M. L. Mashanovitch, *Diode lasers and photonic integrated circuits* (Wiley, 2012).
36. G. Muziol, M. Hajdel, M. Siekacz, K. Szkudlarek, S. Stanczyk, H. Turski, and C. Skierbiszewski, "Optical properties of III-nitride laser diodes with wide InGaN quantum wells," Appl. Phys. Express **12**(7), 072003 (2019).
37. C. Skierbiszewski, G. Muziol, K. Nowakowski-Szkudlarek, H. Turski, M. Siekacz, A. Feduniewicz-Zmuda, A. Nowakowska-Szkudlarek, M. Sawicka, and P. Perlin, "True-blue laser diodes with tunnel junctions grown monolithically by plasma-assisted molecular beam epitaxy," Appl. Phys. Express **11**(3), 034103 (2018).
38. M. Żak, G. Muziol, H. Turski, M. Siekacz, K. Nowakowski-Szkudlarek, A. Feduniewicz-Żmuda, M. Chlipała, A. Lachowski, and C. Skierbiszewski, "Tunnel junctions with doped InGaN quantum well for vertical integration of III-nitride optoelectronic devices," submitted (2020).